3B2v7.51c GML4.3.1 JQI : 714 Prod.Type: com pp.1–13(col.fig.:NIL) ED: H.Ramesh PAGN: ananth SCAN:

ARTICLE IN PRESS

PERGAMON

Quaternary International ▮ (▮▮▮▮) ▮▮▮–▮▮▮

Global ice volume variations through the last glacial cycle simulated by a 3-D ice-dynamical model

R. Bintanja*, R.S.W. van de Wal, J. Oerlemans

Institute for Marine and Atmospheric Research Utrecht, Utrecht University, P.O. Box 80005, 3508 TA Utrecht, The Netherlands

Abstract

A coupled ice sheet—ice shelf—bedrock model was run at 20 km resolution to simulate the evolution of global ice cover during the last glacial cycle. The mass balance model uses monthly mean temperature and precipitation as input and incorporates the albedo—mass balance feedback. The model is forced by the GRIP and Vostok—derived temperature records (and by sea level and solar radiation variations), which are distributed spatially and seasonally. Model simulations show that at the last glacial maximum (LGM) a volume of ice representing about 65 m of sea level equivalent is stored on the Eurasian continent, whereas North America stores 42 m. The other regions (Greenland, Tibet, South-America and Antarctica) contribute about 17 m to global sea level lowering at the LGM compared to present day. Sensitivity experiments show that the ice volumes of the Eurasian and North American ice sheets are particularly sensitive to summer temperature changes. Finally, the timing and mechanism of grounded ice formation and expansion for the last glacial were studied for the Eurasian and North American continents. Ice sheet formation begins at 118 kyr BP in the Barents and Kara Sea region, over Baffin Island and in the high Cordilleran Range following a 4°C cooling. Alternating regions of ice sheet expansion by direct snowfall, ice flow and grounding of ice shelves can be identified. These relate to specific geomorphological traces, and may as such help in model validation.

1. Introduction

At the Last Glacial Maximum (LGM, ~18 kyr BP), the ice sheets over the continents reached their greatest extent of the last glacial cycle. By then, ice stored on land had lowered global sea level by approximately 130 m compared to the present-day level (e.g. Lambeck and Chappell, 2001). In particular the northern hemispheric continents were occupied by huge bodies of ice, none of which exist today: the Laurentide (LIS) and Cordilleran ice sheets (CIS) over North America, and the Fennoscandian (FIS) and Siberian ice sheets (SIS) over Eurasia. The climate of the LGM was characterized by very low temperatures, as deduced from the record of the GRIP ice core in central Greenland (Johnsen et al., 1995) and other proxy data. In fact, temperatures were substantially lower than today during much of the last glacial epoch.

There have been a considerable number of studies in which the ice sheet extent and other features of glacial evolution during the last glacial cycle have been simulated by means of ice sheet models of varying complexity (e.g. Deblonde and Peltier, 1991; Peltier and Marshall, 1995; Marsiat, 1995; Calov and Marsiat, 1998; Greve et al., 1998; Budd et al., 1998), sometimes coupled to a simplified climate model. For instance, Huybrechts and T'siobbel (1997) simulated the LGM ice sheet configuration of the northern hemisphere by an ice sheet model coupled to a climate model of intermediate complexity. They showed good overall agreement between their steady-state ice distribution and the reconstruction of CLIMAP (1976) and Peltier (1994), both in terms of thickness and extent of the ice sheets. However, a drawback of their approach is that they compare their steady-state model output with a real ice sheet configuration that was very probably not in steady state. Another weakness relates to the fact that it is not clear whether the simulated ice sheets will disappear during the deglaciation stage in accordance with the proxy records.

Another approach was followed by Tarasov and Peltier (1997), who presented model simulations over the entire last glacial cycle, that is, inception, build-up and deglaciation of the ice sheets. This is a more appropriate test for an ice sheet model, since there are much more requirements to meet when a full glacial cycle needs to

*Corresponding author. Tel.: +31-30-2533259; fax: +31-30-254-3163.

E-mail address: r.bintanja@phys.uu.nl (R. Bintanja).

1040-6182/02/$ - see front matter
PII: S1040-6182(02)00023-X

be simulated. The timing and magnitude of modelled build-up and retreat stages can be verified against proxy data of the extent (geomorphological evidence), local ice thickness (rebound data) and global ice volume (global sea level changes). Ones aim should be to simulate the volume extent and other characteristics as good as possible, and to identify consistent features in the simulated ice sheet evolutions when model formulations/parameters are varied within their range of uncertainty. Probably the most obvious drawback of this method relates to the difficulty to accurately determine the temperature and especially precipitation forcing. These should either be modelled using a simple climate model or be parameterized, for instance by using general circulation model (GCM) paleoclimate model results.

We will follow the latter approach here. A coupled 3-D thermomechanical ice sheet—bedrock—ice shelf model will be forced with temperature, insolation and sea level data beginning in the Eemian at 120 kyr BP until present. We will present global sea level variations over this period resulting from the formation and disintegration of the various ice sheets around the globe. The focus will be on the ice masses over the North American and Eurasian continents, and the sensitivity of modelled ice volume to changes in model parameters will be investigated. Finally, we investigate the formation/expansion mechanisms of these ice sheets in some detail.

2. Model formulation

The ice sheet model solves the coupled prognostic equations for ice thickness and temperature (e.g. van de Wal, 1999a; Huybrechts, 1990), which are based on the shallow-ice approximation (Hutter, 1993). The 3-D temperature field is governed by diffusion, advection and generation of heat by deformation. The 3-D velocity field is evaluated diagnostically and is determined by deformation and basal sliding. Sliding is set to occur either if (1) the ice temperature at the bed is within 1 K of the pressure melting point, or if (2) grounded ice is bounded by open ocean or ice shelf (the grid point is then part of the grounding line). The equations are solved on a rectangular equidistant grid with a mesh size of 20 km (similar to the ice shelf and bedrock model components), with 10 non-equidistant layers in the vertical. van de Wal (1999a) used this model to simulate the temporal behaviour of the Greenland ice sheet over the last glacial cycle. Table 1 depicts values of model parameters.

The ice shelf model is taken from Oerlemans and van der Veen (1984). It parameterizes ice shelf thickness on an empirical basis, with dynamical aspects being neglected entirely. At each grid point over sea, the ice shelf thickness is assumed to be proportional to the ratio of thickness of the ice at and the distance to the grounding line to a certain power (p), summed over eight radial directions. This procedure favours the formation of ice shelves in (narrow) embayments, in which a large fraction of the local horizon is occupied by grounded ice. The minimum ice shelf thickness is set at 200 m. Moreover, ice shelves are assumed to break up when annual surface air temperatures are over -5°C. Testing the ice shelf model on present-day Antarctic resulted in fairly realistic distributions of the Ronne, Ross and Amery ice shelves for $p = 0.5$, although simulated thicknesses were somewhat too small. Note that the ice-sheet and ice shelf component form a coupled system, since flow of grounded ice is determined partly by the surface slope (which at the grounding line is reduced if an ice shelf is present). Generally, the inclusion of the ice shelf routine leads to a thickening of the grounded ice, especially at the grounding line. Even with a simplistic approach as used here, grounding and ungrounding of the ice sheet—ice shelf system is taken into account, which allow ice sheets to expand across shallow seas in a realistic fashion. Note that changes in sea level may trigger grounding/ungrounding and expansion/retreat in the coupled ice sheet—ice shelf system.

Table 1
Values of model parameters

Parameter	Value
Ice density	$910\,\mathrm{kg\,m^{-3}}$
Heat conductivity of ice	$2.1\,\mathrm{W\,m^{-1}\,K^{-1}}$
Sliding parameter	$0.01\,\mathrm{kPa^{-3}\,yr^{-1}}$
Geothermal heat flux	$0.042\,\mathrm{W\,m^{-2}}$
Flexural rigidity	$4\times10^{22}\,\mathrm{N\,m}$
Relaxation time scale of asthenosphere	3000 yr

We employ a visco-elastic bedrock model to incorporate variations in bed topography resulting from changes in the ice load. The elastic properties of the lithosphere determine the amplitude and spatial pattern of the deflection, whereas the viscous properties of the asthenosphere govern the speed of bedrock adjustment. We therefore use the elastic-lithosphere-relaxing-asthenosphere (ELRA) model of Le Meur and Huybrechts (1996) to simulate bedrock movement. We use global uniform values of the flexural rigidity and the relaxation time scale (Table 1). A detailed description of the bedrock model can be found in Thomassen et al. (2001).

The main input for the model is the present bed topography, assumed to be in local isostatic equilibrium. Changes in sea level are taken relative to the present state. The model domain is subdivided into five possible masks: grounded ice not bordering open sea or ice shelf, grounded ice at the grounding line, ice shelf, open sea and bare rock. Internal model physics determine the

Table 2
Description of the six geographical regions where the model was applied. The latitudinal and longitudinal ranges denote the approximate extent of the model domains, while the final column shows the size of the model grids

Region	Description	Grid size
EAS	Eurasia (10°W–180°E), roughly north of 30° (Europe) and 45° (Asia)	500 × 350
NAM	North-America (50°W–180°W), north of 30°, excluding Greenland	500 × 350
TIB	Tibetan Plateau (60°E–110°E), roughly between 20°N and 45°N	250 × 200
SAM	South-American Andes (0°S–60°S), roughly between 60°W and 80°W	150 × 400
GRL	Greenland	83 × 141
ANT	Antarctica, roughly south of 60°S	281 × 281

state of each grid point at any time. We have defined six regions in which ice sheets may have been present during the last glaciations. These are listed in Table 2. In all simulations a time step of 4 years was used.

3. Mass balance and forcing

The temporal and spatial characteristics of the evolving ice sheets during the last glacial cycle are largely determined by the way in which the surface mass balance is formulated and how the model is forced. We use the present-day distributions of surface air temperature (T, in K) and precipitation from the NCEP reanalysis dataset (Kalnay et al., 1996) as the basic state, which was bilinearly interpolated onto the ice sheet model grid. We use monthly mean values, and henceforth calculate the mass balance in monthly steps. The ablation rate (A, in m w.e. yr^{-1}) is calculated from

$$A = [4(T - T_f) + 0.513(1 - \alpha)Q + b]/100, \quad (1)$$

where $T_f = 273.16\,\mathrm{K}$, Q is the incoming shortwave radiation at the top of the atmosphere (in $\mathrm{W\,m^{-2}}$), and b is a constant ($b = -88$ for ANT and $b = -32$ elsewhere). The various coefficients in (1) were derived from minimizing errors with mass balance observations and results of model runs over Greenland and Antarctica for the present-day climate. In (1), α is the surface albedo, which is determined as

$$\alpha = \min(\alpha_g + 10(\alpha_s - \alpha_g)d, \alpha_s), \quad (2)$$

where α_g is the ground albedo (0.20 for a bare surface and 0.45 for ice), α_s is the albedo of snow (0.80) and d is the snow depth (in m w.e.). Snow depth varies throughout the year, based on the cumulative monthly mass balance, but cannot exceed 10 m w.e. The important elements of this scheme are: (1) it takes into account the effects of seasonal changes in temperature, radiation and precipitation, and (2) it incorporates the albedo—mass balance feedback. Both characteristics are crucially important for the climate sensitivity of glaciers and ice sheets (Oerlemans, 2001), and it strongly affects ice sheet initiation. For instance, large temperature reductions are required to glaciate very dry regions because thin layers of snow have little affect on albedo, which means that the radiation term in (1) remains relatively large and ablation will remain larger than accumulation.

Monthly accumulation of snow is a temperature-dependent fraction of precipitation, the formulation of which is based on data over Greenland (Ohmura et al., 1999). Additionally, changes in the moisture content of air (assumed to be related to precipitation) through changes in temperature are taken into account by using an exponential relation which is an approximation of the Clausius–Clapeyron relation (Huybrechts and T'siobbel, 1997). A result of this is that growing ice sheets will receive less precipitation as they become higher and colder, a process which is sometimes referred to as the elevation-desert effect. The height—mass balance feedback is included since temperature (and with it ablation and accumulation) depends on surface elevation. Note that precipitation changes are applied as fractions of the present-day value, with the present-day temperature as reference. Using GCM data, Rind (1986) showed that the assumption of relative humidity is not a bad assumption for zonally averaged conditions. However, since we will ignore changes in atmospheric dynamics (in particular ice-sheet induced changes in the position of the jet stream) and in the hydrological cycle, some of the important changes in precipitation during the last glacial cycle will not be accounted for.

The model is forced by the temperature records deduced from the GRIP and Vostok ice cores (Jouzel et al., 1993) on the northern and southern hemisphere, respectively. Additionally, we prescribe the spatially and annually varying incident radiation at the top of the atmosphere, caused by slowly varying changes in the Earth's orbital parameters (Berger, 1978), which enter the ablation formulation. Finally, we force the model by global sea level variations (CLIMAP, 1976). In a later stage, we will couple the six regions and allow the coupled model to internally generate global sea level change. However, sea level is probably not a very important factor in determining the evolution of the major ice sheets (except for Antarctica) during glacial cycles, so this will probably not be of great importance.

According to probably all climate models, temperature changes induced by any sort of climate change vary spatially and seasonally. Therefore, it would be unrealistic to apply the GRIP temperature perturbation to the entire Northern Hemisphere and disregard such variations. According to the GISS GCM simulated temperature fields for the present day (PD) and LGM climatic states (Hansen et al., 1983), the temperature

differences between these two climatic states can be categorized into three main effects: (1) temperature changes are dependent on latitude, with the largest differences in the polar regions, (2) temperature changes vary seasonally, with the largest differences occurring during the winter (Fig. 1), and (3) temperature changes are largest over regions covered by land ice. Other models exhibit similar behaviour. On the basis of the GISS GCM output, we have made a parameterization that distributes the ice-core—derived temperature (its deviation from present day, $\Delta T_{\mathrm{icecore}}$) spatially and seasonally:

$$\Delta T = \Delta T_{\mathrm{icecore}} f_s \frac{\zeta}{6}[w(g_1 + g_2\varphi) + (1 - w)g_3 d_m], \qquad (3)$$

where ζ is an amplification factor, φ is latitude (in deg) and d_m (m w.e.) is the annual mean snowdepth, which cannot exceed 10 m w.e. The factor w weighs the effects of latitude and the presence of snow on air temperature. f_s represents seasonal variations in the temperature change (see Fig. 1, bottom panel), and equals the ratio of the monthly mean temperature difference (LGM–PD) and the annual mean difference. Evidently, temperature changes in early summer (May–June) are only 30–35% of the annual value, whereas December exhibits the strongest changes (160%). This is a very important effect, since it implies that decreases in summer temperature (which largely determine annual ablation) were probably much smaller than the average temperature change. However, since these figures are derived from one particular model and can be different in others, we will regard the amplitude (A_s) of seasonal temperature change as a tuning parameter ($A_s = 1$ for the GISS-derived distribution of Fig. 1; $A_s = 0.5$ when the amplitude of change is halved). Incidentally, it is not unlikely that A_s varies spatially and temporally; however, such variations will be ignored here. We also use ζ as a tuning parameter, since there are considerable uncertainties regarding the validity/accuracy of mainly the amplitude of the derived temperatures (e.g. Dahl-Jensen et al., 1998; Cole et al., 1999). The form of the GRIP/Vostok records has not been modified (see Fig. 2). In the standard runs, the model was tuned to produce the correct ice volume at LGM. The values of the various parameters in (3) are taken as follows: $\zeta = 2.8$, $A_s = 0.5$, $w = 0.5$, $g_1 = -1.25$, $g_2 = 0.1021$, $g_3 = 0.27$. Note that the inclusion of d_m in (3) implicitly introduces the effect of the albedo-temperature feedback on temperature. It ensures that ice sheets are colder (and dryer) than their surroundings, even without the elevation-desert feedback.

All simulations described in this paper start at 120 kyr BP, with the present-day bed being in equilibrium with the present-day ice load (of GRL and ANT). Outside these two regions we start with ice-free conditions. Ice sheets can form wherever conditions are favourable; no artificial restrictions or limitations on ice sheet formation or its extent are applied. Note also that the six regions are forced in the same manner; regions were not tuned separately.

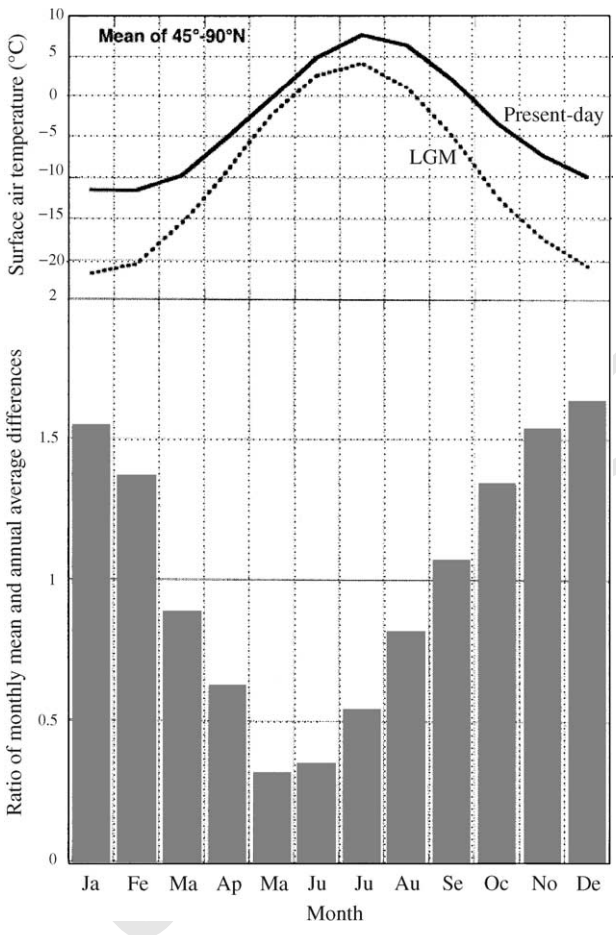

Fig. 1. Surface air temperature in the present-day climate and in the LGM as simulated by the GISS GCM (Hansen et al., 1983) (top). Ratio of the monthly mean temperature difference and the annual mean difference (=6.5°C) (bottom). Values represent means over the area 45°–90°N.

4. Global ice volume variations

In each of the six regions defined in Table 2 a 120 kyr simulation was performed. Fig. 2 shows the simulated ice volume and areal coverage variations. Ice volume was recalculated into equivalent sea level lowering, in order to compare the total value with the observed sea level fluctuations. Evidently, the ice sheets in Eurasia contribute most to sea level lowering, with more than 60 m of sea level equivalent stored at LGM. The North American continent contributes only about two-thirds of that (41 m). This result is in contrast with the LGM reconstruction of Peltier (1994), who found that there was roughly twice as much ice in North America

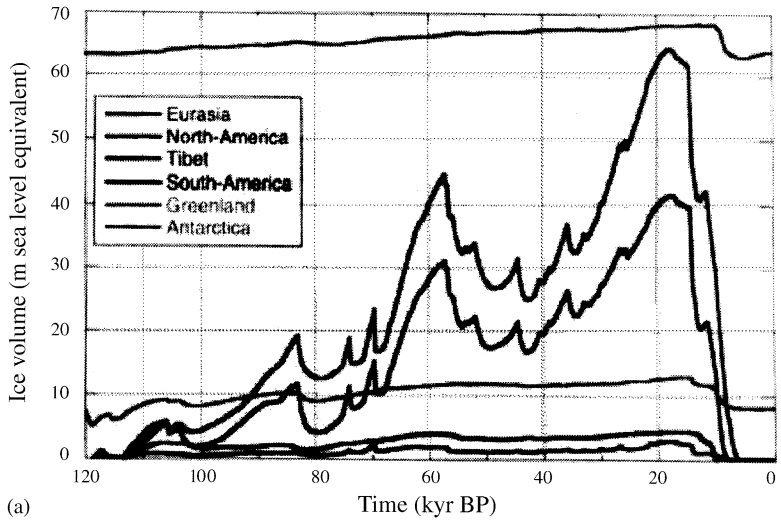

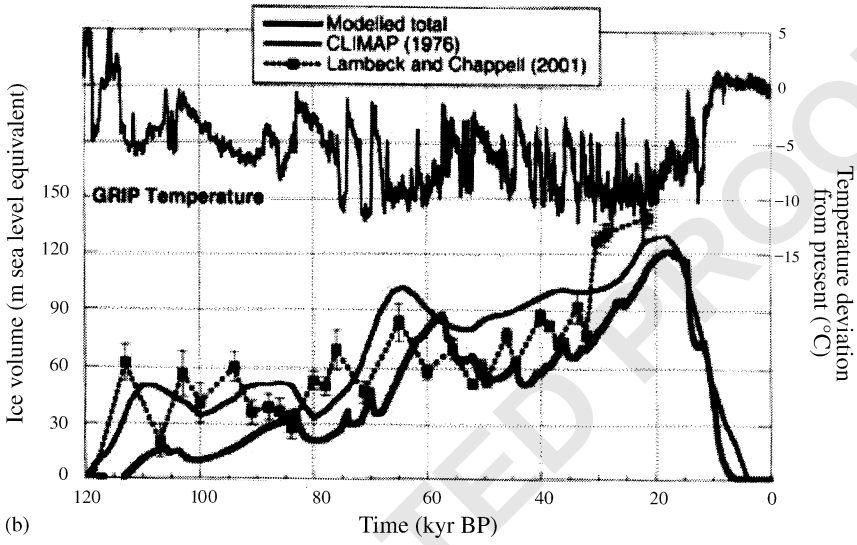

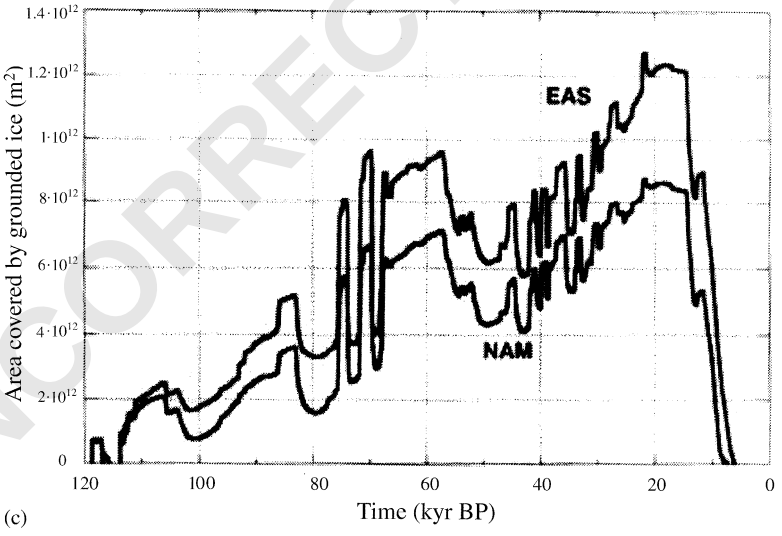

Fig. 2. (a) Variation of simulated ice volume in each of the six regions over the last 120 kyr; (b) total simulated ice volume (deviation from present day) and sea level reconstructions according to CLIMAP (1976) and Lambeck and Chappell (2001), while the GRIP isotope-derived temperature record is shown in black; (c) simulated areal coverage by grounded ice in Eurasia and North America.

Table 3
Simulated values of ice volume in the present day (at the end of a glacial cycle integration) and at the LGM for each of the six regions (in m sea level equivalent)

Region	Present-day ice volume	LGM ice volume
EAS	0.0	64.6
NAM	0.0	41.6
TIB	0.1	3.1
SAM	0.0	4.6
GRL	8.2	12.8
ANT	63.3	68.2
Total	71.6	194.9

compared to Eurasia. Compared to his data, the ice volume in our simulation in Eurasia is overestimated by a factor of three, whereas in North America the ice volume is somewhat too low. Possible reasons for these discrepancies will be discussed in the next paragraphs. Reducing the ice volume over Eurasia by one-third would greatly underestimate global sea level lowering during the entire glacial cycle.

The other four regions exhibit ice sheet formation or extension on a much smaller scale. The volume of the Greenland ice sheet increases by about 50% at LGM, in accord with earlier simulations (e.g. van de Wal, 1999b). In Tibet, two small ice caps form at the southern parts of the high plateau. This seems to be contrasting with the general view that no significant glaciation took place on the Tibetan Plateau during the last glacial cycle, even though some other models also simulate Tibetan ice caps during the last glacial (e.g. Calov and Marsiat, 1998). In South-America, fairly extensive ice fields form in the southern Andes and Patagonia, in accordance with field data. Finally, the Antarctic ice sheet grows steadily during the glacial phase due to the partial grounding of the Ross and Ronne Ice Shelves (a result of sea level lowering), despite the reduction in precipitation caused by the lower temperatures. Also lower ice temperatures, which reduce the viscosity of ice, contribute to the increase in ice thickness. The four regions together contribute 17 m of equivalent sea level (LGM–PD). Table 3 shows the individual contributions of all six regions to sea level lowering at the LGM. The contributions of the six-region sum up to a 123 m global sea level drop at the LGM compared to present-day resulting from the presence of land ice.

Another interesting characteristic of the simulated variations in ice sheet volume can be inferred from Fig. 2a when the EAS and NAM contributions are considered. It relates to the fact that volume variations appear to vary synchronously in both regions. One would perhaps expect that different topographic features induce differences in the dynamic response of the ice sheets. This apparent synchronous behaviour is due to the fact that basically the same temperature forcing was applied to both regions. The variation in total area occupied by grounded ice is shown in Fig. 2c. It shows fast synchronous changes in ice coverage, which can be attributed to the rapid temperature fluctuations in the GRIP data (mainly Dansgaard–Oeschger events). A sudden strong cooling creates a positive mass balance for an extensive region, where a thin ice sheet consequently forms. Most of the short-term fluctuations in volume and especially area can thus be attributed to the rapid temperature fluctuations of the GRIP core data (one might rightfully question whether the rapid GRIP temperature signal should be applied over the entire hemisphere). However, also the longer-term variations in the two regions are quite similar, even though the difference in ice volume at LGM is more than twice as much as at 40 kyr BP. This means that internal dynamic effects contribute to the differences at longer time scales. The overall synchronicity will probably cease to exist when longitudinal variations in temperature forcing are taken into account, as shown by Tarasov and Peltier (1997) who use a 2-D atmospheric energy balance model to drive their ice sheets (even though some of their experiments exhibit a synchronicity similar to that shown in Fig. 2a), or when precipitation changes are (partly) decoupled from temperature perturbations.

The ice sheets in Eurasia and North America both form just after 118 kyr BP at their nucleation centres (as will be discussed in Section 6). After that, they grow to reach peak ice volumes at 85, 60 and 20 kyr BP, interrupted by periods of retreat. Stages of expansion and decline can be linked to relatively cold and warm stages in the GRIP temperature data. This shows that in this model formulation temperature (and with it, precipitation) is the main forcing variable. All ice has disappeared before 6 kyr BP, in accordance with proxy data.

When the simulated total ice volume is compared with global sea level curves derived from proxy data (Fig. 2b), some interesting differences can be inferred. In particular the rate at which ice forms in the period just after the onset of the last glacial (120–110 kyr BP) is difficult to reconcile with the 'observed' sea level curve. The CLIMAP data, recently updated by Lambeck and Chappell (2001), exhibit a sea level drop of more than 50 m within this 10 kyr time period. In contrast, the model produces barely 15 m for all six regions combined, which can for a large part be attributed to the fact that the GRIP temperatures are only slightly lower than present during this period. The model can only be made to produce a sea level drop of 50 m for absurdly large temperature reductions (even if the precipitation is kept at present-day levels), which then result in too much ice during the remainder of the glacial period. A major drop in global (or perhaps regional) temperature, perhaps aided by a precipitation increase, is required to form ice sheets of sufficient volume; at present there is no

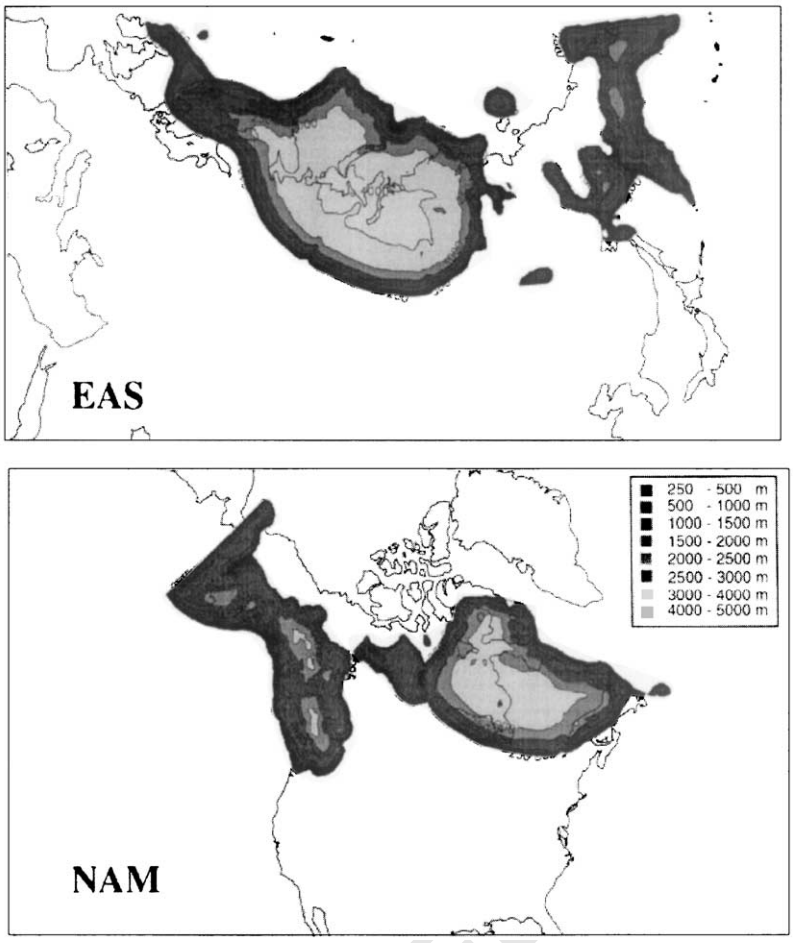

Fig. 3. Geographical distribution of the thickness of grounded ice at the LGM in Eurasia and North America. Note that the Greenland ice sheet is disregarded here.

evidence for such strong temperature reductions at the beginning of the last glacial. We expect that it will be very difficult to match the simulated ice volumes to observed sea level over the entire last glacial cycle, even though the overall form of both profiles (Fig. 2b) agrees reasonably well.

Fig. 3 depicts the ice thickness distribution for EAS and NAM at the LGM. In Eurasia, a major ice sheet has formed over northern Siberia, the Barents and Kara Seas. Maximum ice thickness reaches over 4000 m in the centre. It extends in southwesterly direction over Scandinavia and Scotland, which indicates that the FIS and SIS are just different parts of one major ice sheet. The centre of the SIS/FIS complex lies just south of the Kara Sea, which is a very consistent feature in all our simulations of EAS glaciation. Another consistent feature is that both the FIS ice thickness and the extent seem to be underestimated when compared to geomorphological reconstructions (e.g. Kleman and Hättestrand, 1999). Moreover, the FIS generally forms much later in the glacial cycle (to be discussed in Section 6). Difficulties in simulating early glaciation in Fennoscandia are also reported by Tarasov and Peltier (1997), and appear to be general. They were unable to simulate ice sheets in Scandinavia without imposing additional cooling in the North Atlantic. Experiments with the mass balance model indicate that high central regions of Scandinavia need to be cooled by more than 8°C (relative to present day) to generate a positive mass balance, while only 3–4°C is sufficient for Svalbard and Nova Zembla. The extent of the SIS/FIS complex compares favourably with the simulations of Huybrechts and T'siobbel (1997). There are some ice shelves at the northern boundary of the FIS/SIS, in particular in the embayment north of Nova Zembla. To the east, there appears to be excessive ice in the Kamchatka and Eastern Siberia regions over the wetter coastal regions, but field evidence regarding the extent of glaciation appears to be inconclusive.

In North America, the LIS clearly remains too small, with too little expansion to the south and to the west and northwest (see e.g. Clark et al., 1993). The centre of

the dome lies over Quebec-Labrador and the western Hudson Bay Basin, with maximum ice thicknesses of more than 3000 m. A separate smaller dome is present over Keewatin. There is no connection to the CIS in the west, which occupies much of the coastal region of Canada and southern Alaska. In accordance with geomorphological evidence, northern Alaska remains ice-free (e.g. Clark et al., 1993). The Bering Strait, however, is fully glaciated (the straight edge represents the model domain boundary). The too small volume of LIS and the abundance of ice in the easterly parts of EAS appear to be a more general problem of ice sheet models (e.g. Budd et al., 1998; Calov and Marsiat, 1998). We think that these deficiencies may be attributed to changes in atmospheric transport and the associated changes in precipitation patterns (Greve et al., 1999) that are unaccounted for in the present study.

It is clear why the EAS ice sheets take up a much larger volume than those over NAM in this simulation. In EAS, the simulated ice extent in the Far East is probably not realistic, while in NAM the extent of the LIS is underestimated considerably. The latter may be attributed to the fact that the Canadian Arctic region is perhaps too dry in the present-day state, which means that summer temperatures must decrease significantly for the annual mass balance to become positive (due to the snow-albedo feedback). At the southern margin of the LIS, atmospheric dynamics would be altered due to the presence of the ice sheet with a southward transgression of the jet stream, bringing more precipitation to the southern parts of the LIS. This effect, not included in the present model, would accelerate southward expansion. In the next section we will investigate whether changes in the forcing function can change this overall picture.

5. Sensitivity experiments

In this section we will investigate the effect of changes in the constants that determine the temperature forcing (3) on the temporal evolution of the Eurasian and North American ice sheets. We have varied the values of ζ and A_s, which determine the magnitude of the total temperature forcing and the magnitude of the seasonal cycle, respectively. Fig. 4 shows the volume and areal coverage at LGM as a function of mean temperature for EAS and NAM ice sheets for the various scenarios. The first thing to note is that a decrease in ζ leads to a smaller temperature perturbation and less ice, as would be expected. For instance, decreasing ζ from 2.8 (in the standard run) to 2.1, which relates to a decrease in (surface air) temperature perturbation of more than 7°C, diminishes the amount of ice at LGM to 38 m sea level equivalent for EAS. The changes in ice volume are somewhat less for NAM. In both regions, the rate of change of ice volume per unit temperature change appears to be fairly linear for the range of ζ-values considered.

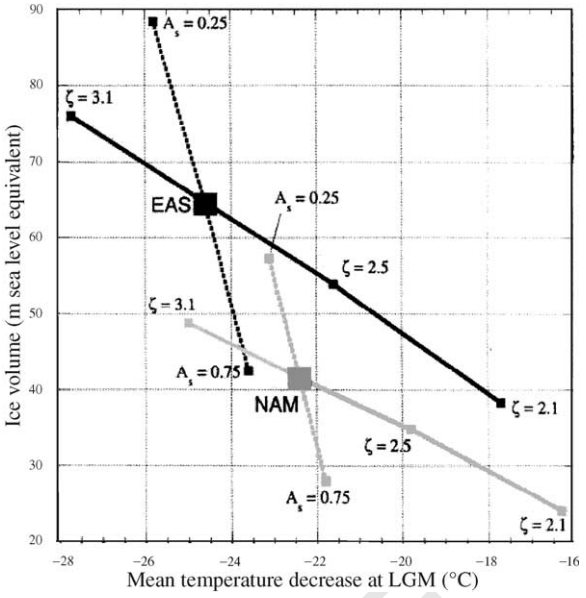

Fig. 4. Dependence of modelled ice volume at the LGM for different values of ζ and A_s, which determine the magnitude and seasonal amplitude of the temperature forcing, respectively, on the surface air temperature decrease at LGM averaged over the model domains. Eurasian values are in black, while North American values are in grey. The big squares represent values for the standard experiment ($\zeta = 2.8$ and $A_s = 0.5$).

Obviously, a change in ζ similarly affects temperatures in all seasons. To investigate the effect of changes in the seasonal cycle of temperature, we have changed the value of A_s to 0.25 and 0.75 (its value in the standard run is 0.5). An increase in A_s means that the amplitude of the seasonal temperature change is increased, so that winters get colder and summers warmer. Especially its effect on summer temperature is important, as can be inferred from Fig. 4. An increase of A_s to 0.75 leads to drastic reductions in ice volume, even though the mean temperature increases only slightly (mainly due to the decrease in ice surface elevation, and to the last term in the forcing function (3)). The higher summer temperatures cause extensive ablation and a reduction of surface albedo, thereby reducing ice thickness and extent. Similarly, a lower value of A_s causes strong increases in ice volume due to lower summer temperatures. The rate of volume change per unit temperature change seems to be similar for both regions.

Generally, the volume changes caused by changes in the values of ζ and A_s are governed by the dependence of ablation on temperature, and hence by the albedo—mass balance feedback. The non-linear nature of this feedback mechanism prevents easy interpretation of the changes in regional ice extent. In any event, very dry regions such as the northern Canadian Arctic islands

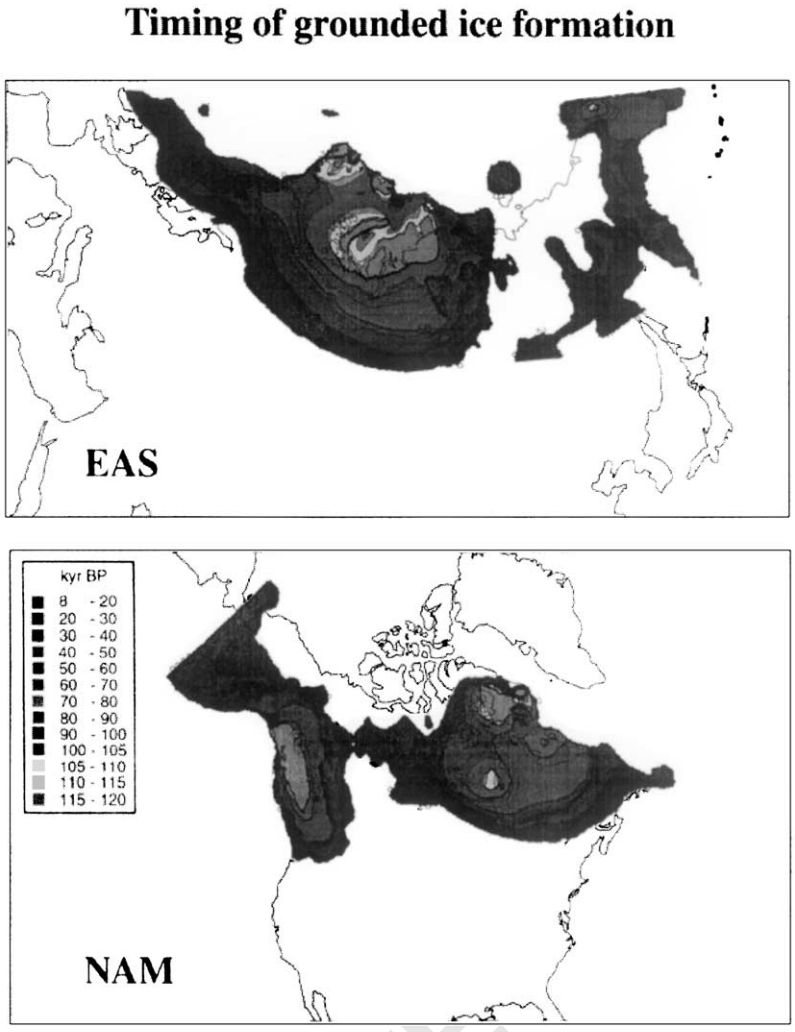

Fig. 5. Geographical distribution of the timing of grounded ice 'formation' in Eurasia and North America. It shows the timing of the first occurrence of grounded ice at any location within the model domain.

remain free of ice even for the strongest forcing considered here.

6. Mechanisms and timing of ice sheet formation

In this section we will investigate the inception and temporal evolution of the EAS and NAM ice sheets in some detail. In the standard runs discussed in Section 4, the timing of first glaciation (that is, the first occurrence of grounded ice) was stored for each model grid box using the following rules: ice must remain for at least 1 kyr to be regarded a real initiation (to prevent fast fluctuations in forcing from disturbing the picture), and if ice disappears values are reset and a later glaciation is stored when the intervening period without ice cover lasts at least 10 kyr. Furthermore, the process by which this grounded ice was 'formed' is of interest. In the current model, grounded ice can 'form' at any location in three different ways:

1. The mass balance becomes positive, so that snow can accumulate to form ice. Any body of ice has to begin in this manner.
2. Ice flows in from a neighbouring grid box. This can (and often will) happen while the local mass balance is still negative.
3. A previously floating ice shelf grounds, and becomes part of the ice sheet.

The model was set to record, which of these three mechanisms was responsible for the first occurrence of grounded ice at each individual grid point.

Figs. 5 and 6 show the spatial distribution of timing and mechanism of grounded ice formation in EAS and NAM, respectively, for the standard runs discussed in Section 4. In Eurasia, the ice initially forms in Svalbard, Franz Josef Land, Nova Zembla and the coastal regions of the Kara Sea. The 4° temperature drop at 118 kyr BP resulted in a positive mass balance in these regions. When these first ice sheets became sufficiently thick, ice

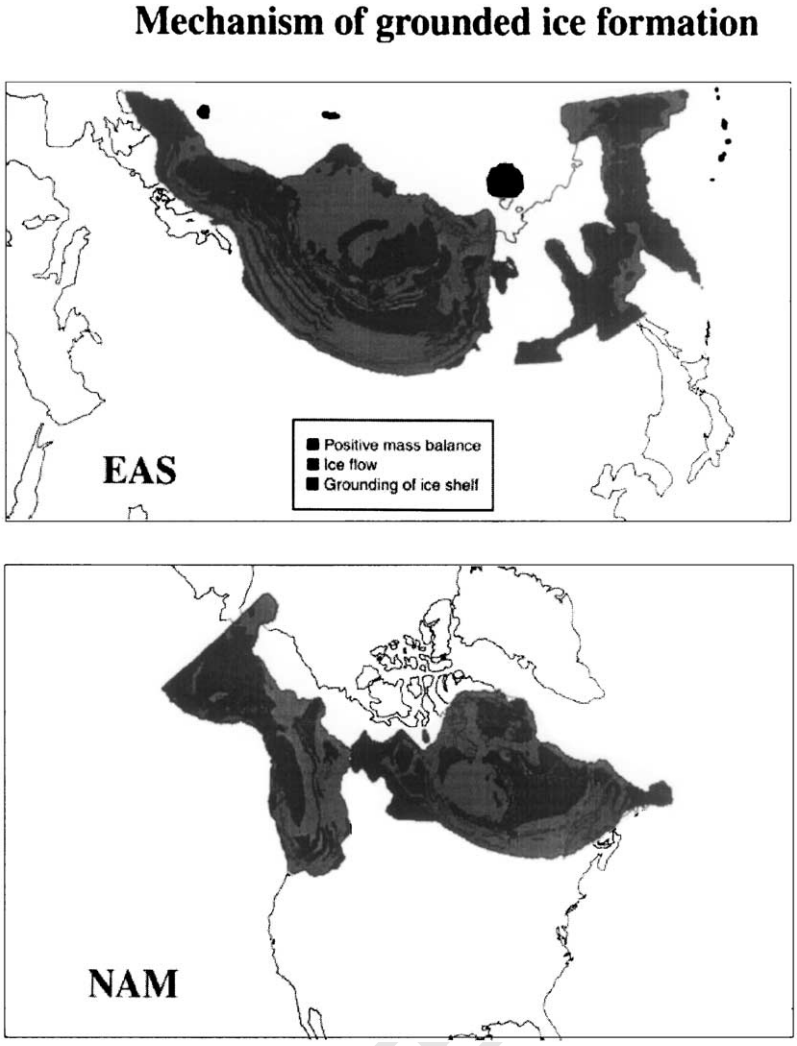

Fig. 6. Geographical distribution of the mechanism by which grounded ice 'formed' in Eurasia and North America (see text). It shows by which of the three mechanisms the ice sheet forms or expands.

shelves progressively covered the Kara and Barents Seas. These eventually grounded, which combined the separate domes into one major ice sheet (SIS) centreed over the Barents Sea (Fig. 5). By 80 kyr BP, this entire region was entirely covered by ice. This formation sequence occurs very consistently in all model runs. Most of this ice sheet was 'formed' by the grounding of ice shelves, which demonstrates the importance of incorporating an ice shelf routine. In contrast, most other modelling studies simply allow the ice sheet to expand towards the continental shelf edge (e.g. Tarasov and Peltier, 1997), which will most likely lead to a significantly different ice sheet evolution.

After 80 kyr BP, the SIS expanded almost exclusively in a southward direction. As can be inferred from Fig. 6, this expansion was not gradual at all. During strong cooling stages, ice expanded owing to the fact that the mass balance in regions adjacent to the ice sheet became positive (blue regions). During periods of less intense cooling, the main ice sheet grew more steadily by means of ice flowing southward (green regions). In several regions a close alternation of these stages can be observed. When the main ice sheet stopped expanding or even retreated somewhat during relative warm stages (such as at 80 and 60 kyrs BP, see Fig. 2) the bed under and adjacent to the main ice body became depressed due to the load of the ice sheet. When such quasi-stationary phases last sufficient long, the bed along the margin can become depressed below sea level. This resulted in the formation of elongated proglacial lakes in which the main ice sheet calved. In a following cooling phase these lakes were covered again by ice shelves, which subsequently grounded to become part of the main ice body (red regions). The existence of several of these elongated proglacial lakes can be identified from Fig. 6, and some may have even been connected to the ocean. Evidently, the mechanism by which ice sheets expand determines to a great extent the geomorphological traces that are left behind. For instance, stages in which ice flow dominates expansion are likely related to the formation of

moraines. Therefore, we anticipate that such information can be used to constrain ice-flow model output when compared with geomorphological evidence.

Ice sheet expansion over Scandinavia occurred relatively late (the northernmost parts became glaciated at 70 kyr BP, whereas the south did not become ice covered before 30 kyr BP). As mentioned before, this contradicts with the proxy evidence that suggests that northern Scandinavia became glaciated as early as 110 kyr BP. Additional early regional cooling seems to be required to account for this discrepancy. Analyses at sediment cores taken in the North-Atlantic ocean suggest that this may indeed have occurred (e.g. Cortijo et al., 1994), and climate models predict additional polar cooling as a result of a retardation of the ocean thermohaline circulation (e.g. Bintanja and Oerlemans, 1996). Most of the interior of Scandinavia, as well as parts of the (dry) North Sea and Scotland became glaciated by means of a positive mass balance (incidentally, this does obviously not rule out the possibility that subsequent ice flow can scour the surface). The continental shelf regions off western Norway became glaciated through grounding of ice shelves.

In North America, similar ice sheet expansion features can be observed. Ice nucleation occurred over the high and western parts of the Cordilleran, the southern parts of Baffin Island, northern Quebec-Labrador and in the eastern part of the (dry) Hudson Bay at 118 kyr BP. The first two regions are very consistent nucleation centres in all model runs. No ice forms on Ellesmere Island, in contrast with most modelling studies (e.g. Marshall and Clarke, 1999). The coupled general circulation—ice sheet model simulation for 116 kyr BP of Pollard and Thompson (1997) showed ice sheet inception nuclei situated mainly on Baffin Island but also on Ellesmere Island. As mentioned before, the northern Arctic Islands of Canada are probably too dry to become glaciated in our model. With regard to the CIS, most expansion took place through outward (easterly) ice flow, interrupted by narrow regions in which ice was formed through a positive mass balance under intense cooling stages. Southern Alaska became glaciated relatively late (around 50 kyr BP), mostly by a positive mass balance or grounding of ice shelf. There is a nucleation centre at 90 kyr BP over the Bering Strait, which can also be identified in the EAS figure. Regarding the LIS, the Hudson Bay and the straits around Baffin Island became rapidly filled with ice shelves, which eventually grounded and merged the separate domes at 60 kyr BP. Interestingly, in this simulation the mainland of Quebec-Labrador became glaciated both from the west and from the north, with narrow regions where the expansion processes of mass balance and ice flow alternate. Note the expansion during the Younger Dryas (the only cooling period in the period 20–8 kyr BP) in purple (Fig. 5), which occurred mostly as grounding of the ice shelves in proglacial lakes to the south and west of the Hudson Bay region. The same feature can be detected near the southernmost margin of the SIS in EAS.

The question now is: how consistent are the various features depicted in Figs. 5 and 6? If the entire picture would change considerably for a small change in some model variable, then there is little use in discussing small-scale details and trying to use this in relating model output to geomorphological evidence. Evidently, we need to look for features that show up consistently (some of which have already been mentioned above). We have examined output from the sensitivity runs discussed in the previous section. In particular, we have looked closely to simulations in which the total ice volume was larger than in the standard run, for instance the perturbation run in which ζ was set to 3.1. The most interesting aspect of this simulation is that the geographical patterns of formation/expansion mechanisms remain virtually similar to those depicted in Figs. 5 and 6 for both EAS and NAM, with only few differences in the fine details. Also, the alternating pattern of expansion mechanisms remains the same, with only their geographical location being slightly shifted away from the ice sheet centre in case of stronger forcing when the ice sheet expansion was faster.

The absence of any significant change in the timing and mechanism of ice sheet initiation/expansion when model parameters are varied should not be taken to imply that these patterns remain the same for any change in the model. However, they do indicate that the distribution of timing and mechanisms of ice sheet inception are robust model results for the simulations presented in this paper. We expect that some features of the model simulations, such as the formation of the ice sheet in the Barents and Kara Seas region, will prove to be very robust.

7. Conclusions

A coupled 3-D ice sheet—ice shelf—visco-elastic bedrock model (20 km resolution) was developed to simulate global ice volume variations during the last glacial period. The model is forced by monthly and spatially varying fields of temperature and precipitation deviations from the present-day values using the GRIP and Vostok temperature records, and by solar radiation and sea level variations. Precipitation changes are taken to be dependent of temperature only by using an approximation of the Clausius–Clapeyron relation. The mass balance model evaluates ablation and accumulation rates, and snow cover, on a monthly basis, which therefore includes the albedo—mass balance feedback. The distribution function of the temperature forcing was deduced from general circula-

tion model output for the LGM and present day. The main feature of this is that the temperature forcing is largest near the poles and in winter, and reduced during the summer. This is important, since the summer temperature determines to a large extent whether the winter snow can survive through the summer.

Six regions were defined in which ice volume variations were simulated over the glacial period (120 kyr BP until present): Eurasia, North America, Greenland, Tibet, South-America, and Antarctica. The focus was on the first two regions. The most important findings are summarized below.

1. In the standard run, the amount of ice stored in Eurasia is about 65 m of sea level equivalent at the LGM, whereas in North America only 41 m is present. The four other regions together contribute 17 m to global sea level lowering.
2. The simulated Laurentide ice sheet centres over eastern Labrador, and remains too small compared to geomorphological reconstructions (e.g. Clark et al., 1993). There is probably too much ice in the far east of Siberia.
3. The volume of ice in Eurasia and North America varies synchronously, which can probably be attributed to the way the ice sheets are forced (e.g. precipitation is related to temperature perturbations). The model is unable (by far) to simulate the 50 m of sea level lowering between 120 and 110 kyr BP that is suggested by proxy evidence; this is one of the features most difficult to simulate correctly in transient experiments. In the present model formulation, absurdly large temperature reductions would be required to induce such a rapid build-up of land ice.
4. Experiments with changed forcing parameters indicate that the amount of grounded ice depends strongly on the imposed change in the amplitude of the annual temperature cycle (specifically summer temperature).
5. In Eurasia, inception of the ice sheet took place on the islands and coasts in the Barents and Kara Sea region. These merged by means of ice shelf grounding in the continental shelf sea to form a major ice sheet at 70 kyr PB. This ice sheet subsequently expanded southward and over Scandinavia. In North America, ice sheet formation starts in the high Cordilleran Range, over central Baffin Island and in the northern parts of Quebec-Labrador. These results agree qualitatively with the GCM results for 115 kyr BP of Dong and Valdez (1995) in the sense that the nucleation centres are in the same regions.
6. Three different mechanisms by which grounded ice can 'form' have been identified: snow accumulation when the mass balance is positive, ice flow from adjacent regions and the grounding of ice shelves. Ice sheet expansion occurred by one of these mechanisms, depending on the rapidity and duration of the air temperature fluctuations. The geographical distribution of the occurrence of these mechanisms shows distinct patterns of alternating expansion mechanisms. The mechanism of ice formation determines to a large extent the geomorphological traces that are left behind. Therefore, they can be used to link model output to geomorphological evidence.

Evidently, the model and especially the forcing formulations should be further refined so that better agreement is obtained with the available proxy evidence. An interesting check to the model is to compare computed bedrock movement with local uplift data in the vicinity of ice sheets (Lambeck and Chappell, 2001). The most useful way to gain insight in paleo-ice sheet evolution using this type of model is to try to define features that show up consistently in the various model simulations. Also coupling of the ice sheet model with a (necessarily simplified) climate model seems to be a fruitful way to proceed.

Acknowledgements

We are indebted to Martijn Thomassen for allowing us to use his bedrock model, and for discussions about ice sheet dynamics. Piet Jonker kindly assisted in getting over several computational hurdles. The constructive reviews of R. Calov and R. Greve are highly appreciated. Financial support was provided by the Netherlands organization of Scientific Research (NWO), in the framework of the PULS funding programme of the Earth and Life Sciences department (ALW).

References

Berger, A., 1978. Long term variations of daily insolation and quaternary climate changes. Journal of Atmospheric Sciences 35, 2362–2367.

Bintanja, R., Oerlemans, J., 1996. The effect of reduced ocean overturning on the climate of the last glacial maximum. Climate Dynamics 12, 523–533.

Budd, W.F., Coutts, B., Warner, R.C., 1998. Modeling the Antarctic and Northern Hemisphere ice-sheet changes with global climate through the glacial cycle. Annals of Glaciology 27, 153–160.

Calov, R., Marsiat, I., 1998. Simulations of the Northern Hemisphere through the last glacial-interglacial cycle with a vertically integrated and a three-dimensional thermomechanical ice-sheet model coupled to a climate model. Annals of Glaciology 27, 169–176.

Clark, P.U., et al., 1993. Initiation and development of the Laurentide and Cordilleran ice sheets following the last interglaciation. Quaternary Science Reviews 12, 79–114.

CLIMAP Project members, 1976. The surface of the ice-age earth. Science 191, 1131–1137.

Cole, J.E., Rind, D., Webb, R.S., Jouzel, J., Healy, R.J., 1999. Global controls on interannual variability of precipitation $\delta^{18}O$: The

relative roles of temperature, precipitation amount, and vapor source region. Journal of Geophysical Research 104, 14223–14235.

Cortijo, E., Duplessey, J.C., Labeyrie, L., Leclaire, H., Duprat, J., van Weering, T.C.E., 1994. Eemian cooling in the Norwegian Sea and North Atlantic ocean preceding continental ice-sheet growth. Nature 372, 446–449.

Dahl-Jensen, D., et al., 1998. Past temperatures directly from the Greenland ice sheet. Science 282, 268–271.

Deblonde, G., Peltier, W.R., 1991. Simulations of continental ice sheet growth over the last glacial-interglacial cycle: experiments with a one-level seasonal energy balance model including realistic topography. Journal of Geophysical Research 96, 9189–9215.

Dong, B., Valdez, P.J., 1995. Sensitivity studies of Northern Hemisphere glaciation using an atmospheric general circulation model. Journal of Climate 8, 2471–2496.

Greve, R., Wyrwoll, K., Eisenhauer, A., 1999. Deglaciation of the Northern Hemisphere at the onset of the Eemian and Holocene. Annals of Glaciology 28, 1–8.

Hansen, J., Russell, G., Rind, D., Stone, P., Lacis, A., Lebedeff, S., Reudy, R., Travis, L., 1983. Efficient three-dimensional global models for climate studies. Monthly Weather Review 111, 609–662.

Hutter, K., 1993. Theoretical Glaciology: Material Science of Ice and the Mechanics of Glaciers and Ice Sheets. Reidel Publ. Co., Dordrecht, 510pp.

Huybrechts, P., 1990. A three-dimensional numerical model for the Antarctic ice sheet: a sensitivity study on the glacial-interglacial contrast. Climate Dynamics 5, 79–92.

Huybrechts, P., T'siobbel, S., 1997. A three-dimensional climate-ice sheet model applied to the last glacial maximum. Annals of Glaciology 25, 333–339.

Johnsen, S.J., Dahl-Jensen, D., Dansgaard, W., Gundestrup, N.S., 1995. Greenland temperatures derived from GRIP borehole temperature and ice core isotope profiles. Tellus 47B, 624–629.

Jouzel, J., et al., 1993. Extending the Vostok ice-core record of paleoclimate to the penultimate glacial period. Nature 364, 407–412.

Kalnay, E., et al., 1996. The NCEP/NCAR 40-year reanalysis project. Bulletin of the American Meteorological Society 77 (3), 437–471.

Kleman, J., Hättestrand, C., 1999. Frozen-bed Fennoscandian and Laurentide ice sheets during the last glacial maximum. Nature 402, 63–66.

Lambeck, K., Chappell, J., 2001. Sea level change through the last glacial cycle. Science 292, 679–686.

Le Meur, E., Huybrechts, P., 1996. A comparison of different ways of dealing with isostacy: examples from modelling the Antarctic ice sheet during the last glacial cycle. Annals of Glaciology 23, 309–317.

Marshall, S.J., Clarke, G.K.C., 1999. Ice sheet inception: subgrid hypsometric parameterization of mass balance in an ice sheet model. Climate Dynamics 15, 533–550.

Marsiat, I., 1995. The waxing and waning of the Northern Hemisphere ice sheets. Annals of Glaciology 21, 96–102.

Oerlemans, J., 2001. Glaciers and Climate Change. Balkema, Lisse, 148pp.

Oerlemans, J., van der Veen, C., 1984. Ice Sheets and Climate. Reidel, Dordrecht, 217pp.

Ohmura, A.P., Calanca, Wild, M., Anklin, M., 1999. Precipitation, accumulation and mass balance of the Greenland ice sheet. Zeitschrift für Gletscherkunde und Glazialgeologie 35, 1–20.

Peltier, W.R., 1994. Ice age paleotopography. Science 265, 195–201.

Peltier, W.R., Marshall, S.J., 1995. Coupled energy-balance/ice-sheet model simulations of the glacial cycle: a possible connection between terminations and terrigenous dust. Journal of Geophysical Research 100, 14269–14289.

Pollard, D., Thompson, S.L., 1997. Driving a high-resolution dynamic ice-sheet model with GCM climate: ice-sheet initiation at 116,000 BP. Annals of Glaciology 25, 296–304.

Rind, D., 1986. The dynamics of warm and cold climates. Journal of Atmospheric Science 43, 3–24.

Tarasov, L., Peltier, W.R., 1997. Terminating the 100 kyr ice age cycle. Journal of Geophysical Research 102, 21665–21693.

Thomassen, M., van de Wal, R.S.W., Oerlemans, J., 2001. The present-day imbalance of the Antarctic ice sheet. Journal of Geophysical Research, submitted for publication.

Wal van de, R.S.W., 1999a. The importance of thermodynamics for modeling the volume of the Greenland ice sheet. Journal of Geophysical Research 104, 3887–3898.

Wal van de, R.S.W., 1999b. Processes of buildup and retreat of the Greenland ice sheet. Journal of Geophysical Research 104, 3899–3906.